PHILOSOPHICAL TRANSACTIONS OF THE ROYAL SOCIETY A MATHEMATICAL, PHYSICAL & ENGINEERING SCIENCES

# The DELPHI Experiment

P. S. L. Booth

*Phil. Trans. R. Soc. Lond. A* 1991 **336**, 213-222
doi: 10.1098/rsta.1991.0074

# The DELPHI experiment

By P. S. L. Booth

*Oliver Lodge Laboratory, Department of Physics, Oxford Street, University of Liverpool, Liverpool L69 3BX, U.K.*

The DELPHI experiment is designed to study in detail the final state particles produced in electron–positron collisions at LEP. The detector has $4\pi$ acceptance with emphasis on three-dimensional information, particle identification, high granularity and precise vertex determination. The detector and its performance during its first year of operation is described.

## 1. Introduction

The DELPHI detector (a detector with lepton, photon and hadron identification) has been operating at LEP since the first electron–positron collisions in August 1989. The detector is designed to have a $4\pi$ acceptance with particular emphasis on three-dimensional information, high granularity, precise vertex determination provided by silicon strip detectors and particle identification provided by ring imaging Cherenkov detectors (RICHes). Apart from the RICHes and the tracking detector for the luminosity monitor (SAT), all other sub-detectors have been fully operational since LEP start-up.

During the first year of LEP operation, DELPHI (Aarnio *et al.* 1991) has recorded 138000 hadronic decays of the $Z^0$, corresponding to an integrated luminosity of 6.3 $pb^{-1}$. Figure 1 shows examples of typical event displays.

DELPHI is situated 100 m underground at intersection point 8 on the LEP ring. Figure 2 shows a perspective view of DELPHI. The main features are a cylindrical barrel section and two endcaps. With the end-caps closed, the detector is self-shielding, allowing access to the electronics and sub-detector computers housed in local control rooms on both sides of DELPHI. Compressed data are transmitted via an optical link to the main computer and control centre on the surface.

The superconducting solenoid, of length 7.4 m and inner diameter 5.2 m, produces a magnetic field of 1.2 T parallel to the beam axis with an excellent homogeneity, necessary for the long-drift detectors (TPC, HPC, barrel-RICH).

In the following discussion, a coordinate system with the $z$-axis parallel to the beam, radius $R$ and azimuth $\phi$ in the plane perpendicular to it and polar angle $\theta$ ($= 0$ along $z$) is assumed.

## 2. Tracking detectors

Charged particle tracking in the barrel region is provided by the vertex detector (VTX), inner detector (ID), time projection chamber (TPC), outer detector (OD) and barrel muon chambers (BMU). In the end-cap regions, tracking is provided by forward chamber A (FCA), forward chamber B (FCB) and forward muon chambers (FMU).

*Phil. Trans. R. Soc. Lond.* A (1991) **336**, 213–222
*Printed in Great Britain*

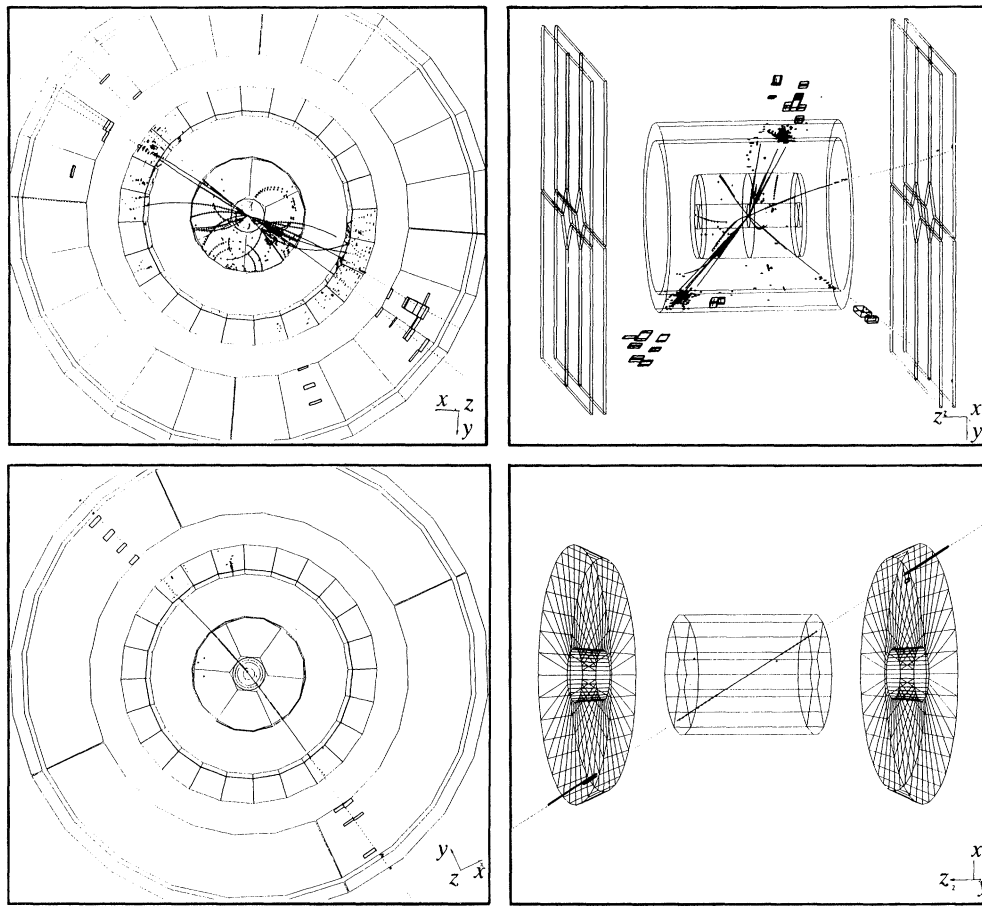


Figure 1. Examples of $Z^0$ events, as seen on the DELPHI interactive graphics display.

### (a) *Vertex detector* (VTX)

The VTX (Chabaud *et al.* 1990) consists of two concentric shells of Si-strip detectors at average radii of 9 and 11 cm surrounding the aluminium beam pipe (outer radius 7.9 cm, thickness 1.2 mm) and covers the range $43° \leqslant \theta \leqslant 137°$.

The purpose of the VTX is to provide maximum $R\phi$ resolution to permit good vertex reconstruction, particularly important for the study of heavy flavour physics. Figure 3 shows a schematic diagram of the assembly of the two shells. Each shell consists of 24 modules with 10% overlap in $\phi$ between the modules. Each module consists of four detectors along $z$ with strips parallel to the $z$-axis. Detector pairs are wire-bonded in series and read out at each end. Individual Si-detectors (sensitive length 59 mm, width 25.6 mm/32 mm for inner/outer shell) are 300 μm thick with a diode pitch of 25 μm and analogue read-out at 50 μm pitch. The total number of read-out strips for the VTX is 54.2 K. Preliminary internal alignment with tracks from $Z^0$ events has given $\sigma_{R\phi} = 14$ μm/point for the full VTX.

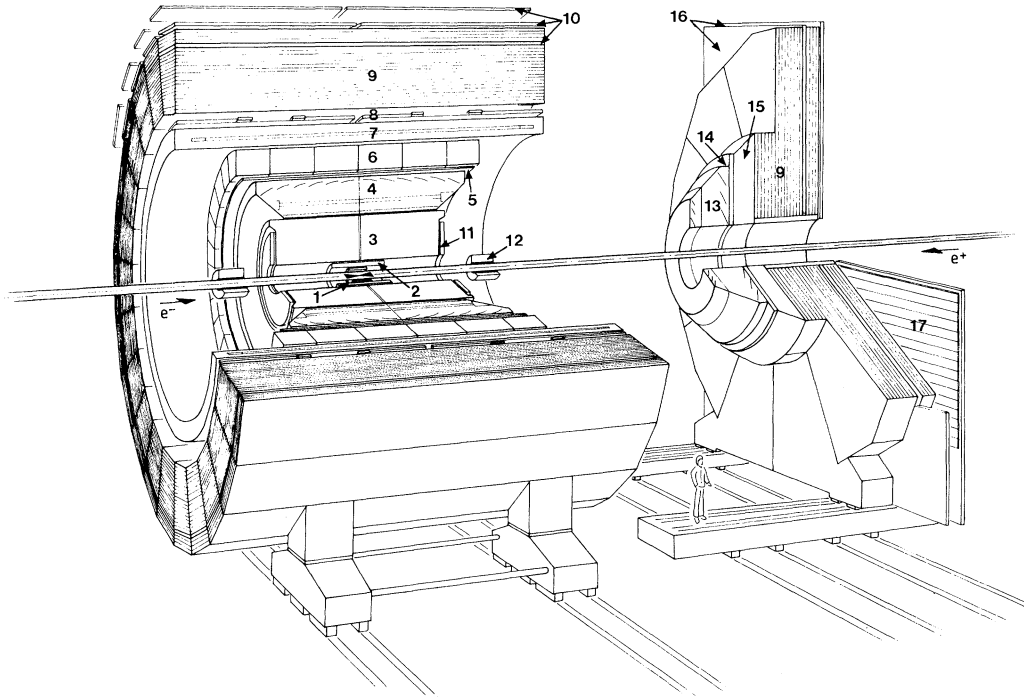


Figure 2. Perspective view of the DELPHI detector. (1) Vertex detector, (2) inner detector, (3) time projection chamber, (4) barrel-RICH, (5) outer detector, (6) high density projection chamber, (7) solenoid, (8) time of flight counters, (9) hadron calorimeter, (10) barrel muon chambers, (11) forward chamber A, (12) small-angle tagger, (13) forward RICH, (14) forward chamber B, (15) forward electromagnetic calorimeter, (16) forward muon chambers, (17) forward hodoscope. The very small angle tagger falls out of view.

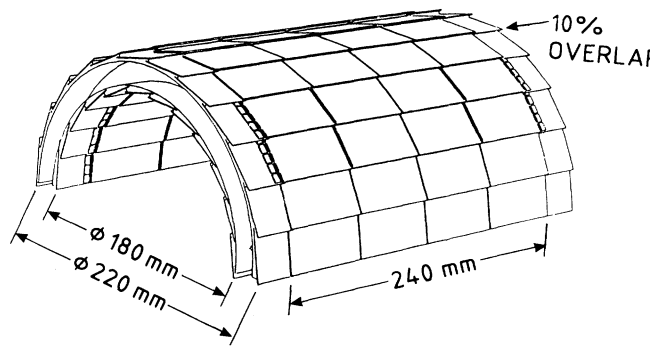


Figure 3. Sketch of the assembly of half of the vertex detector, indicating 10% overlap between 15° sectors.

### (*b*) *Inner detector* (ID)

The ID (Hartjes *et al.* 1987), which provides high redundancy for vertex reconstruction and trigger information, consists of two concentric layers: an inner drift chamber with jet-chamber geometry, giving 24 $R\phi$ points per track; and five

cylindrical multiwire proportional chamber (MWPC) layers which give fast $R\phi$ and $z$ trigger information and solve left/right ambiguities in the jet section.

During LEP running, the average single wire resolution is $\sigma_{R\phi} = 90$ μm in the jet section and $\sigma_z = 1$ mm in the outer layers.

### (c) *Time projection chamber* (TPC)

The TPC (Brand *et al.* 1989) is the principal tracking device in DELPHI, providing three dimensional charged particle position information and $\mathrm{d}E/\mathrm{d}x$ measurements for particle identification. Due to the presence of the barrel-RICH, the size of the TPC is limited ($R_{\max} = 120$ cm, $L = 2 \times 150$ cm) and consequently other tracking detectors (OD, FCA, FCB) are included to improve momentum resolution.

The TPC consists of two identical halves, symmetric about $\theta = 90°$, each filled with $\mathrm{Ar/CH_4}$ (80/20 %) at 1 atm. pressure (*ca.* $10^5$ Pa). A longitudinal electric field (150 V $\mathrm{cm^{-1}}$) is produced in the gas by a high voltage plane at $\theta = 90°$ and a field cage, producing an electron drift velocity of 67 mm $\mu\mathrm{s}^{-1}$. Each end-cap is divided into six sector plates, each plate having 192 sense wires (providing $\mathrm{d}E/\mathrm{d}x$ information) and 16 circular pad rows with constant spacing (providing space point information). Individual pad dimensions are typically 8 mm × 8 mm.

Preliminary results during LEP operation are: $\sigma_{R\phi} = 180$–$280$ μm, depending on $\phi$ and $z$; $\sigma_z < 0.9$ mm; two-track separation = 1.5 cm. The $\mathrm{d}E/\mathrm{d}x$ resolution is at present $\sigma = 6.2\,\%$ for muons at 45 GeV and 7.5 % for pions between 280 and 400 MeV (before pulse height calibration of the wires).

### (d) *Outer detector* (OD)

The OD (Amery *et al.* 1989) provides fast trigger information in both $R\phi$ and $z$ and significantly improves the momentum resolution for high momentum tracks in the barrel region.

The OD ($R_{\min} = 197$ cm, $R_{\max} = 208$ cm) is composed of 24 modules, mounted on the barrel-RICH, each 4.7 m long and consisting of 145 drift tubes arranged in five layers. The layers are staggered and overlap with adjacent modules to provide full azimuthal coverage. The drift tubes are operated in the limited streamer (LS) mode. All layers provide $R\phi$ information and three layers provide fast $z$ trigger information by relative timing of signals from each end of the drift tube. Performances during LEP running are: $\sigma_{R\phi} = 110$ μm/point and $\sigma_z = 4.4$ cm/point.

### (e) *Barrel muon chambers* (BMU)

The BMU detector is composed of two layers. The first layer of $2 \times 24$ modules is installed in the magnet return yoke after 90 cm of iron and consists of three staggered drift chamber planes (2 + 1 spare). The second layer is mounted on the outside of the yoke, behind a further 20 cm of iron and consists of two staggered planes of drift chambers. The chambers operate in the proportional mode and $z$ information is provided by delay line read-out. Individual chamber efficiencies of about 95 % have been recorded during LEP running and measurements of resolution on extrapolated tracks give $\sigma_{R\phi} = 4$ mm and $\sigma_z = 2.5$ cm at present.

### (f) *Forward chambers* (FCA *and* FCB)

FCA and FCB provide powerful tracking and triggering over the range $11° \leqslant \theta \leqslant 33°$.

FCA is mounted on both ends of the TPC. Each side consists of three chambers, turned with respect to each other by 120°, each chamber having two staggered layers




PHILOSOPHICAL TRANSACTIONS OF THE ROYAL SOCIETY A MATHEMATICAL, PHYSICAL & ENGINEERING SCIENCES

providing $2 \times 3$ coordinates ($xx'$, $uu'$, $vv'$, where $x'$ is staggered with respect to $x$). The chambers are operated in the LS mode and preliminary results at LEP give $\sigma = 300$ μm per layer.

FCB provides a precise track element for triggering, pattern recognition and improved momentum resolution. The chambers are mounted between the FRICH and FEMC and each consists of 12 sense wire planes rotated in pairs by 120° with respect to each other providing $2 \times (xx', uu', vv')$. The chambers are operated in the proportional mode and results at LEP yield $\sigma_x = \sigma_y = 130$ μm.

### (*g*) *Forward muon chambers* (*FMU*)

Both arms of the FMU detector have two planes of chambers. The first plane is inside the magnet yoke behind more than 85 cm of iron and the second is behind a further 20 cm of iron, outside the yoke. Each plane, covering $9 \times 9$ m$^2$ is composed of four quadrants, a quadrant consisting of two orthogonal layers of 22 drift chambers. The chambers are operated in the LS mode and coordinates are derived from anode drift times and delay line read-out. Using halo muons, preliminary resolutions $\sigma_x = \sigma_y = 3$ mm have been achieved at LEP.

### (*h*) *Combined tracking*

Precise alignment of the individual tracking detectors is essential for optimum momentum resolution. This is achieved by calibration with high statistics $Z^0$ events and is an ongoing process. To date the following results have been obtained for muon pairs at 45.6 GeV: $dp/p = 7\%$ in the barrel region (combining ID, TPC, OD) and $dp/p = 12\%$ in the forward region (combining ID, TPC, FCB).

## 3. Scintillation counters

Two sets of scintillation counters TOF and HOF provide fast trigger signals for both $Z^0$ events and cosmic ray calibration events.

### (*a*) *Time-of-flight counters* (*TOF*)

The TOF system consists of a single layer of 172 counters mounted just outside the solenoid and covering the range $41° \leqslant \theta \leqslant 139°$. Time resolution with cosmics is $\sigma_t = 1.2$ ns, corresponding to $\sigma_z = 20$ cm and detection efficiency is 99.9% for minimum ionizing particles (MIP(S)). The excellent time resolution allows the TOF data to be used off-line to veto cosmic ray muons in time with beam crossings.

### (*b*) *Forward hodoscopes* (*HOF*)

The HOF are mounted on each side between the end-cap yoke and the second layer of the FMU chambers and cover an area of 140 m$^2$ in a single layer. The layer is arranged in four quadrants, each containing 28 counters. Detection efficiency is greater than 95% for MIPs with a time resolution of 5 ns. The HOF is used primarily to trigger on di-muon events and beam halo muons used for alignment.

## 4. Electromagnetic calorimeters

### (*a*) *High density projection chamber* (*HPC*)

The HPC (Navarria 1987) applies the time projection principle to calorimetry and measures the three-dimensional charge distribution induced by electromagnetic showers and by hadron showers with high granularity in all coordinates. The time projection principle is realized by using the lead converter as the electric field cage.




PHILOSOPHICAL TRANSACTIONS OF THE ROYAL SOCIETY A MATHEMATICAL, PHYSICAL & ENGINEERING SCIENCES

Figure 4

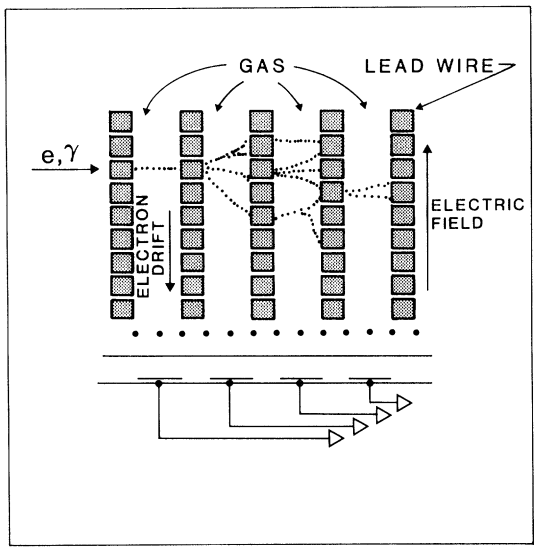


Figure 5

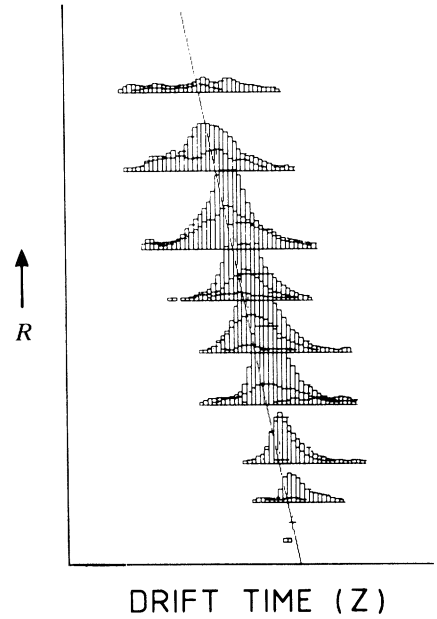


Figure 4. Schematic diagram of the HPC principle.

Figure 5. HPC samples obtained from a 45 GeV electron shower.

The ionization charge is drifted onto a single proportional wire plane at one end of the HPC module.

The principle of operation of the HPC is shown in figure 4. The converter consists of 41 lead walls spaced by 8 mm gaps. Each layer is formed by thin lead wires insulated from each other. A voltage gradient between neighbouring lead wires provides a longitudinal drift field of about 100 V $cm^{-1}$ in the $Ar/CH_4$ (80/20) gas mixture, corresponding to an electron drift velocity of *ca.* 5 cm $\mu s^{-1}$.

The proportional chambers use pad read-out, where the pad pattern defines the granularity of radial and azimuthal coordinate sampling (1° in $\phi$ and nine-fold sampling in $R$ over $18X_0$). The $z$ coordinates is derived from the drift time with a granularity of 4 mm.

A plane of scintillators is installed in one of the HPC gaps at a depth of $4.5X_0$ to provide a fast trigger.

The HPC detector consists of 144 separate modules and is mounted inside the solenoid and covers the range $43° \leqslant \theta \leqslant 137°$. Calibration can be checked with α-sources installed in each module and by the periodic use of a minute admixture of radioactive Kr gas emitting 40 keV photons.

From test beam data on shower axis reconstruction, the angular resolution of the HPC alone is $(36/\sqrt{E}+2.5)$ mrad in $\theta$ and $(97/\sqrt{E}+10)$ mrad in $\phi$, with an energy resolution measured to be $\sigma_E/E = (23/\sqrt{E}+1.1)\,\%$.

All HPC modules have operated reliably since LEP start-up. Figure 5 shows HPC samples for a 45 GeV Bhabha electron shower.

### (*b*) *Forward electromagnetic calorimeter* (*FEMC*)

The FEMC (Checcia *et al.* 1989) is designed to have a good energy resolution and granularity. Each arm consists of a 5 m diameter disc with a total of 4532 lead glass blocks in the form of truncated pyramids, arranged to point at the interaction point. The FEMC covers the ranges $10° \leqslant \theta \leqslant 36.5°$ and $143.5° \leqslant \theta \leqslant 170°$.

Individual blocks ($20X_0$ deep) are read out by vacuum phototriodes. At DELPHI, the energy resolution is degraded due to about $2X_0$ of material in front of the FEMC. Bhabhas at 45 GeV were measured with $\sigma_E = 4\,\%$ and $\sigma_\theta = 0.3°$.

### (*c*) *Small angle tagger* (*SAT*)

The SAT is the main luminosity monitor in DELPHI and measures small-angle Bhabha events. Each arm consists of a calorimeter behind a silicon tracker (tracker yet to be implemented). The calorimeter, covering $2.5° \leqslant \theta \leqslant 7.7°$, consists of alternating layers of 0.9 mm thick lead sheets and plastic scintillating fibres, aligned parallel to the $z$-axis. The total depth of the calorimeter is $28X_0$ and the fibres are read our via light-guides by photodiodes.

Until the trackers are commissioned, the inner acceptance radius is defined to better than 100 μm by a precision lead mask ($10X_0$) in front of one calorimeter. The energy resolution of 45 GeV electrons is $\sigma_E = 4.4\,\%$ and the impact point is determined to 2 mm. The experimental systematic error on luminosity determination is estimated to be 0.8 % at present. There is an additional 0.5 % systematic error from uncertainties in the theory.

### (*d*) *Very small angle tagger* (*VSAT*)

The VSAT is a Bhabha luminosity monitor at very small angles and has a Bhabha rate about 10 times greater than the SAT. It provides a fast monitor of the luminosity and machine operation and is an independent check of the SAT measurements.

The detector in each arm is composed of two rectangular W–Si calorimeter stacks, $24X_0$ deep, 5 cm high, 3 cm wide and 10 cm long. The stacks are mounted at $|z| = 7.7$ m on both horizontal sides of the beam pipe and cover polar angles $5 \leqslant \theta \leqslant 7$ mrad and an azimuth of 45° around the horizontal axis.

Each stack consists of 12 W-plates interleaved with full area Si detectors for energy measurement. Two Si-planes with 32 vertical strips (1 mm pitch) at depths of $5X_0$ and $9X_0$ and one plane of 48 horizontal strips at $7X_0$ are used to eliminate showers at the detector edge and to correct for lateral energy leakage. The energy resolution for 45 GeV electrons is 5 %.

## 5. Hadron calorimeter (HCAL)

The HCAL is a sampling gas detector incorporated in the magnet yoke. In both the barrel and end-cap regions, layers of limited streamer tubes are inserted into 2 cm slots between the 5 cm thick iron plates of the yoke (20/19 layers in the barrel/end-cap regions) providing complete $4\pi$ coverage. The calorimeter contains 19032 individual tubes with pad readout. Pads are shaped to form towers pointing at the interaction point and typically pads of five adjacent layers are combined electrically into a tower. Each tower covers an angular region $\Delta\phi \approx 3.7°$ and $\Delta\theta \approx 2.8°$. The analogue signals from the towers are available both for triggering and off-line analysis.

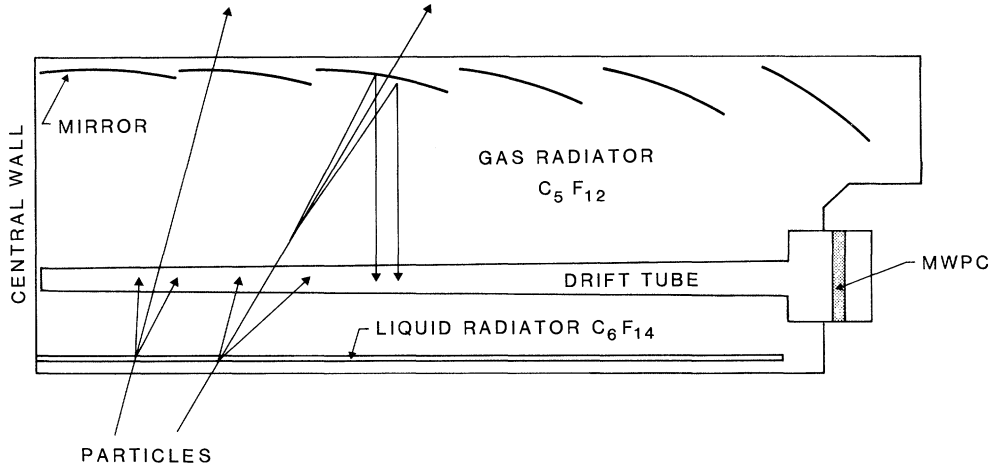


Figure 6. Schematic diagram of a sector of the barrel-RICH.

After solving initial severe noise problems, HCAL has operated very reliably at LEP. The performance has been studied using both hadronic and di-muonic events from $Z^0$ decays. The hadronic energy response is linear and the resolution is about $120\%/\sqrt{E}$. The HCAL alone can distinguish hadronic decays of the $Z^0$ from background. The efficiency of single muon detection in the barrel for 45 GeV muons from dimuon decay of the $Z^0$ is measured to be around 80%.

## 6. Ring imaging Cherenkov counters (RICH)

An important feature of DELPHI is the use of RICHes to aid hadron identification over a wide momentum range by Cherenkov angle reconstruction from both liquid and gas radiators. The design aims are for $4.2\sigma$ separation for $\pi$/K up to 18 (30) GeV/$c$ and for K/p up to 33 (50) GeV/$c$ in the barrel (forward) RICH.

### (*a*) *Barrel-RICH*

The barrel-RICH (Arnold *et al.* 1988), which covers the angular region $41° \leqslant \theta \leqslant 139°$, is shown in figure 6. A charged particle crosses a gaseous and a (1 cm thick) liquid radiator where Cherenkov photons are emitted at angle $\theta_c$ to the track direction ($\cos\theta_c = 1/\beta n$: $n$ = refractive index, $\beta = v/c$). Parabolic mirrors focus the photons from the gaseous radiator backward onto a photosensitive gas contained in quartz tubes; the photons from the liquid radiator travel 12 cm and hit the same photon detector from below. The photosensitive gas is ionized by the photons, the Cherenkov light cone leaving a 'charge image' in the gas. Using the time projection principle, the electrons of the 'charge image' are drifted to a MWPC at one end of the quartz drift tube, allowing three-dimensional coordinates of the conversion points of the Cherenkov photons to be measured. Consequently $\theta_c$ and $\beta$ can be determined. Particle identification is achieved by using the momentum of the particle, determined from the combined tracking, as additional information.

The barrel-RICH consists of two identical halves about $\theta = 90°$, each segmented azimuthally into 15° sectors. Each sector contains a liquid radiator, quartz drift tube + MWPC, six mirrors and the gas volume. The liquid ($C_6F_{14}$) and gas ($C_5F_{12}$)

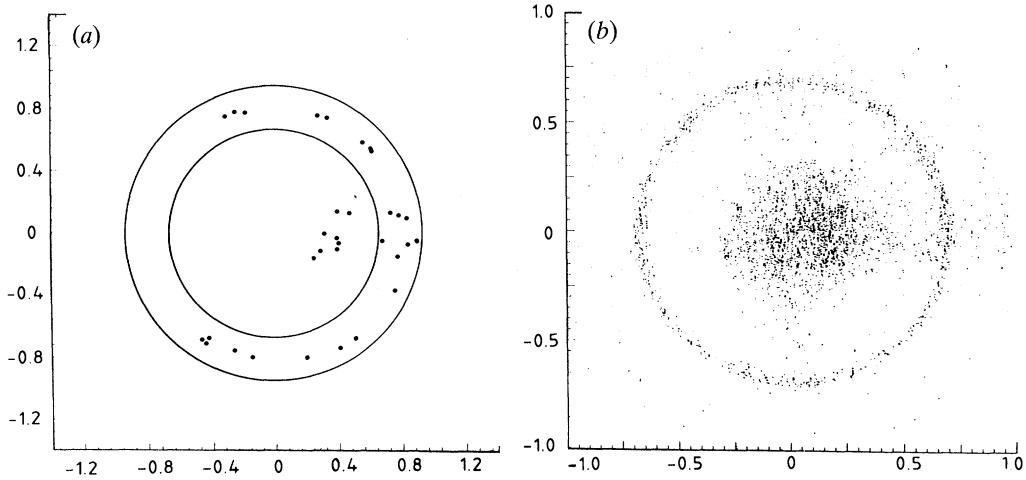


Figure 7. Rings obtained with the liquid radiator for the barrel-RICH. (*a*) From a single high momentum particle. (*b*) Superposition of photons from 45 GeV muons.

radiators are chosen to minimize the gap between the ranges of particle identification. The drift gas ($CH_4/C_2H_6$ 75/25 %) is doped (0.1 %) with the photo-sensitive agent TMAE. The operating temperature of the detector is 40 °C. This is necessary since $C_5F_{12}$ is liquid at room temperature and the increased temperature allows a higher TMAE concentration.

All the barrel-RICH components were installed for the start up of LEP, except for the drift tubes in one half-cylinder (installed autumn 1990). The first results were obtained using only the liquid $C_6F_{14}$ liquid radiator. Figure 7*a* shows a result of a single high momentum track. Due to total reflection at the liquid radiator surface, only part of the ring is observed. Superimposed rings from many muon pairs are shown in figure 7*b*. The error on the measured Cherenkov angle $\sigma_\theta = 14$ mrad, contains an appreciable contribution from extrapolation errors on the particle tracks, to be eliminated after proper tuning and alignment. The average number of photo-electrons per liquid ring is $\langle N \rangle = 12$. These data were obtained with an effective TMAE temperature of 11 °C and are in accordance with the prototype result $\langle N \rangle = 18$ for TMAE at 30 °C.

Very preliminary results from the gas-radiator were obtained near the end of the 1990 LEP operation. Since the detector was operating at ambient temperature, $C_2F_6$ was used as a test radiator. For dimuonic events, $\sigma_\theta = 6$ mrad and $\langle N \rangle = 2.1$ were obtained, in good agreement with Monte Carlo studies.

The barrel-RICH is expected to be operating at design specification for the start of the next LEP operation in Spring 1991.

### (*b*) *Forward-RICH*

The forward-RICH is mounted in each end-cap region in front of the FEMC. Each detector consists of two truncated half-cones and is divided azimuthally into 12 modular sectors. Each sector contains one driftbox, two MWPCs, three liquid-radiator containers and five mirrors. The MWPCs are mounted radially on the two borders of each 30° sector. Operation is foreseen with $C_5F_{10}$ and $C_6F_{12}$ as gas and liquid radiators and $C_2H_6$ + TMAE as drift gas.




PHILOSOPHICAL TRANSACTIONS OF THE ROYAL SOCIETY A MATHEMATICAL, PHYSICAL & ENGINEERING SCIENCES

Prototype test beam studies gave $\langle N \rangle = 20/10$ for the liquid/gas radiators. So far at LEP, only one 30° sector of one end-cap is installed, priority having been given to the barrel-RICH.

## 7. The trigger system

The DELPHI four-level trigger system (Aarnio *et al.* 1991) is designed to cope with high luminosities and possible high background rates. The first and second trigger levels are synchronous with the beam cross over (BCO every 22 μs) with trigger decisions 3 μs and 40 μs after BCO respectively. The third and fourth level triggers are asynchronous with respect to BCO. During LEP operation so far, with a luminosity of a few $\times 10^{30}$ cm$^{-2}$ s$^{-1}$, and the low background levels experienced at LEP, trigger rates were typically 500 Hz at first level and 2–3 Hz at second level. It was unnecessary to implement third and fourth level triggers. Redundancy of the various trigger components allowed the detailed study of trigger efficiencies for both hadronic and leptonic events. The read-out system is based on the Fastbus standard.

## 8. Summary

During the first year of LEP operation, DELPHI has recorded 138000 hadronic $Z^0$ decays with trigger rates about 2.5 Hz at the highest luminosities achieved of $5 \times 10^{30}$ cm$^{-2}$ s$^{-1}$. All sub-detectors apart from the RICHes have been operational and many sub-detectors have already reached their design performance, permitting a rapid analysis of the physics channels available at LEP.

## References

Aarnio, P., *et al.* 1991 The DELPHI Detector at LEP. CERN-PPE/90-128. *Nucl. Instrum. Meth.* A. (Submitted.)

Amery, A., *et al.* 1989 The DELPHI outer detector. *Nucl. Instrum. Meth.* A **283**, 502–508.

Arnold, R., *et al.* 1988 A ring imaging Cherenkov detector. The DELPHI barrel RICH prototype. *Nucl. Instrum. Meth.* A **270**, 255–318.

Brand, C., *et al.* 1989 The DELPHI time projection chamber. *Nucl. Instrum. Meth.* A **283**, 567–572.

Chabaud, V., *et al.* 1990 Beam test results from a prototype for the DELPHI microvertex detector. *Nucl. Instrum. Meth.* A **292**, 75–80.

Checchia, P., *et al.* 1989 Performance of the forward electromagnetic calorimeter (FEMC) for the end caps of the DELPHI detector. *Nucl. Instrum. Meth.* A **275**, 49–58.

Hartjes, F., *et al.* 1987 A drift chamber with variable drift velocity. *Nucl. Instrum. Meth.* A **256**, 55–64.

Navarria, F. 1987 Some aspects of the DELPHI HPC project. *Nucl. Instrum. Meth.* A **257**, 499–508.





PHILOSOPHICAL TRANSACTIONS OF THE ROYAL SOCIETY A MATHEMATICAL, PHYSICAL & ENGINEERING SCIENCES